ARTICLE

# Turbulence Spectra for Boundary-Layer Winds in Tropical Cyclones: A Conceptual Framework and Field Measurements at Coastlines

**Lixiao Li · Ahsan Kareem · Julian Hunt · Yiqing Xiao · Chaoying Zhou · Lili Song**

**Abstract**  A conceptual model is proposed for the characteristic sub-ranges in the velocity and temperature spectra in the boundary layer of tropical cyclones (hurricanes or typhoons). The model is based on observations and computation of radial and vertical profiles of the mean flow and turbulence, and on the interpretation of eddy mechanisms determined by shear (namely roll and streak structures near the surface), convection, rotation, blocking and sheltering effects at the ground/sea surface and in internal shear layers. The significant sub-ranges, as the frequency increases, are associated with larger energy containing eddies, shear and blocking, inertial transfer between large and small scales, and intense small-scale eddies generated near the surface caused by waves, coastal roughness change, and the buoyancy force associated with the evaporation of spray droplets. These sub-ranges vary with the locations at which the spectra are measured, i.e. the level $z$ in relation to the height $z_{max}$ of the peak mean velocity and the depth $h$ of the boundary layer, and the radius $r$ in relation to the eyewall radius $R_{ew}$ and the outer-vortex radius $R_{ov}$. For two tropical cyclones (Nuri and Hagupit), experimental data were analyzed. Spectra were measured where $r$ is near to $R_{ew}$ and $R_{ov}$ using four 1-h long datasets at coastal towers, at 10- and 60-m heights for tropical cyclone Nuri, and at 60-m height for tropical cyclone Hagupit at the south China coast. The field measurements of spectra within the boundary layer show significant sub-ranges of self-similar energy spectra (lying between the length scale 1,000 m and the smallest scales less than 40 m) that are consistent with the above conceptual model of the surface layer. However, with very high wind speeds near the eyewall, the energy of the independently

L. Li · Y. Xiao · C. Zhou
Shenzhen Graduate School, Harbin Institute of Technology, Shenzhen 518055, China

A. Kareem (✉)
NatHaz Modeling Laboratory, University of Notre Dame, Notre Dame 46556, USA
e-mail: kareem@nd.edu

J. Hunt
Institute of Disaster Reduction, University College London, London WC1E 6BT, UK

L. Song
Public Meteorological Service Center, China Meteorological Administration, Beijing 10081, China

generated intense surface eddy motions, associated with surface waves and water droplets in the airflow, greatly exceeds the energies of the small scales in the inertial sub-range of the boundary layer, over scales less than about 3–40 m depending on the height $z$ and the radius $r$. This rise in the small-scale frequency weighted spectra ($nS_u(n)$, where $n$ is natural frequency, and $S_u(n)$ is the energy spectrum of the longitudinal wind component) is consistent with the hypothesis that these processes are only weakly correlated with the main boundary-layer turbulence.

**Keywords** Boundary layer · Field measurements · Tropical cyclone · Turbulence spectrum · Velocity profile

## 1 Introduction

In the boundary layer of tropical cyclones (hurricanes or typhoons), the mean and turbulent wind fields have characteristic flow structures driven by buoyancy and shear that are observed to vary significantly as the radius $r$ increases from near the eyewall radius $R_{ew}$ (i.e. $r \approx R_{ew} \approx 20$ km) to the outer-vortex regions of radius $R_{ov}$ ($r \approx R_{ov} \approx 400$ km) of the tropical cyclone. These mean flow and turbulence structures are significant, both from a meteorological and from a structural engineering viewpoint because they affect the overall dynamics of tropical cyclones (Emanuel 1986; Lighthill 1998; Chan 2005; Paget 2009) and determine the mean and fluctuating wind forces on buildings and other structures. Currently, most estimates of these forces are similar to those computed in the neutrally stratified boundary layer over flat terrain, and make use of standard relations for the wind-speed profile, spectra and probability distributions (e.g. ESDU 2007), as was noted at the ICSU/WMO meeting in Beijing in 1992. However, since then, many studies have shown that the structure of turbulent boundary layers at high wind speeds can be very different from the standard von Karman spectrum, especially in the large wavenumber range; the peak of the normalized spectrum $nS_u(z, n)/\sigma_u^2$ either shifted to a low frequency or a high frequency range (e.g. Kaimal and Finnigan 1994; Högström et al. 2002; Schroeder and Smith 2003; Caracoglia and Jones 2009; Zhang 2010). The variance of wind fluctuations in tropical cyclones also exceeds those observed in extratropical storm boundary-layer flows that are largely shear driven near the surface. The main mechanisms are attributed to the influences of deep convection above the surface layer and downbursts (Collier and Thome 1994), and the effects of blocking of large eddies by variable mean shear near the ground or sea surface (Smedman et al. 2004). Because these dynamical effects influence the eddy structure and the time scale of the eddies, the changes in the forms of the spectra for the horizontal and vertical wind fluctuations over different sub-ranges can either be derived by approximate theories based on rapid distortion or surface eddy concepts, combined with the familiar Kolmogorov–Obukhov scaling laws for the inertial sub-range (following Townsend 1976; Hunt 1984; Mann 1994; Hunt and Carlotti 2001). For these boundary layers, the airflow and eddying motions generate waves, and transport droplets and salt particles into the air, which not only affects the thermodynamics, but also the turbulence (Barenblatt et al. 2005). Because these small-scale motions are larger than, and statistically independent of, the smallest eddies of the inertial sub-range turbulence driven by shear and convection above the surface layer, their spectra can be simply added to the spectra of boundary-layer turbulence (see Townsend 1976). The intensity of these surface eddying processes is dominated by the way that salty droplets are carried upwards and many kilometres inland where they contaminate irrigation and farmlands (Fitzroy 1863).

The spatial distribution and intensity of the detailed fluid processes at different heights and radii in tropical cyclones can be studied using robustly constructed meteorological towers on the coasts where tropical cyclones frequently make landfall. The detailed spectra measured on such towers enabled the effects of spray on the thermodynamics, as well as the dynamics of turbulence in the surface regions of tropical cyclones, to be analyzed for the first time. Another important aspect of tropical cyclones considered here is the difference in the turbulence structure between the front sector of the whole tropical cyclone (denoted here as forward F regions) and the rear sector of the whole tropical cyclone (denoted as backward B regions). For example, convection and lightning are stronger in the F regions than in the B regions (Hall et al. 1992).

New measurements of the wind profiles and turbulence spectra in tropical cyclones presented here, using recently commissioned observation towers in China, provide a closer look at the various spectral sub-ranges and delineate features of turbulence structure that are both similar and different to those in the lower atmosphere away from the tropical cyclone. Computational models of the mean flow presented by Paget (2009) show that, near the eyewall, the vertical profiles of the mean azimuthal velocity, $U$, have a local maximum value at a height of around 40–100 m above the ocean surface. Since $U$ also decreases with radius $r$ over a distance of order $R_{ew}$, the mean flow structure in the lower part of the tropical cyclone is significantly different from that of the unidirectional atmospheric boundary layer over a flat surface. Rapid distortion theory shows how an unsteady shear flow moving over an area of strong convection leads to a low-level jet in the mean flow, which is caused by the very strong convective turbulence dominating the shear turbulence near the surface (Owinoh et al. 2005).

A remarkable feature of a tropical cyclone's flow field is the very sharp gradient of mean flow and turbulence at the eyewall, (seen from aircraft and satellites), similar to the sharp turbulent/non-turbulent interfaces at the edges of free shear flows and boundary layers (Hunt et al. 2006). The sharp interface/eyewall meets the ground and the radial pressure gradient associated with the turbulence gradient (Townsend 1976) drives an inward flow, which stimulates roll structures that are aligned with the swirling flow by the combined convective and dynamic instabilities (Foster 2005). These are also driven by other kinds of disturbance in turbulent boundary layers, such as buoyant convection (Smedman et al. 2007).

Previous research on these roll structures has been reported by Wurman and Winslow (1998) showing that the wind shear can cause strong periodicity with scales around 500 m or smaller (Lorsolo et al. 2008). The boundary-layer rolls also magnify the ratio of the variation of longitudinal fluctuating velocity to friction velocity in tropical cyclones (Masters et al. 2010; Li et al. 2012) and other flows with convective turbulence (Smedman et al. 2007).

## 2 Flow Mechanisms and Concepts for the Different Locations and Scale Ranges of the Spectra

Schematic diagrams of the production processes affecting turbulence at different levels near the eyewall ($r \approx R_{ew}$) and the outer-vortex regions ($r \approx R_{ov}$) are shown in Fig. 1a and Fig. 1b. Boundary-layer roll structures oriented parallel to the mean velocity (in red in Fig. 1b) bring high momentum air to the surface, which results in horizontal wind shear at scales around 500 m (Wurman and Winslow 1998). Figure 1b shows even smaller rolls (in green), with wind shear at smaller scales (sub-rolls) resulting in quasi-periodic damage patterns. Similar observations have been reported in Wurman and Winslow (1998).

**(a)**



**(b)**
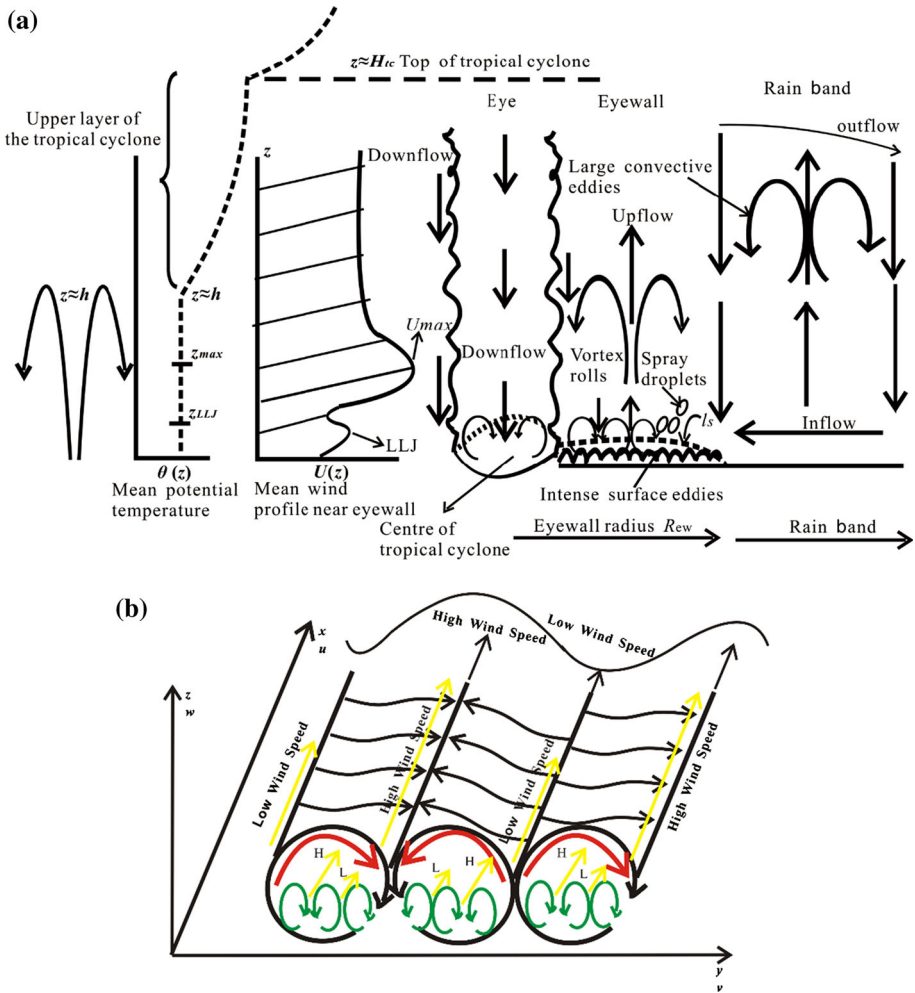


**Fig. 1** Sketches of the flow structure of a tropical cyclone: **a** mean flow structure and turbulence dynamics near eyewall and outer-vortex regions; and **b** vortex structure in the eyewall region (H means high wind speed, and L means low wind speed). LLJ is the low-level jet

Table 1 summarizes the characteristics of tropical cyclone turbulence dynamics and mean flow structures at various heights according to the findings of previous studies. From this table and studies of turbulence dynamics in the planetary boundary layer (PBL), a conceptual model of turbulence spectra in tropical cyclone is developed below.

The different length scales of these processes largely determine the different components of the energy spectra $E_{ii}$, which have characteristic forms over wavenumber ($k$) or frequency ($n$) (noting that $k = 2\pi n U^{-1}$) weighted spectral sub-ranges corresponding to the relevant physical length scales (see Fig. 2). The spectra also vary between the different layers defined above, and between different radii in the tropical cyclones. In Fig. 2, the longitudinal spectra $E_{11}$ in the convective boundary layer (Hunt 1984) and in the surface layer of a neutral boundary layer (Hunt and Morrison 2000) are also included to show the similarities and differences with the spectral model in tropical cyclone wind field.

**Table 1** Characteristics of tropical cyclone turbulence dynamics at different levels

| Levels | Turbulence dynamics |
| --- | --- |
| $z = H_{tc}$ | Top of the tropical cyclone (typically $H_{tc} \approx 5-10$ km). Turbulence is cloud-driven convection (but mean temperature profile is slightly stable) |
| $z = h$ | Top of the tropical cyclone boundary layer (when $r \approx R_{ew}$, $h \approx 500-1{,}000$ m; when $r \approx R_{ov}$, $h \approx 1{,}000$ m) |
| | Note that $h$ is smaller than the height of the planetary boundary layer because of higher Coriolis forces and stronger mean stratification above $z \approx h$ |
| $z_{max} < z < h$ | In the upper layer of tropical cyclones, turbulence is driven by buoyant convection. Its structure is in the form of isolated plumes growing upwards, with smaller plumes feeding into them near their base irrespective of surface processes (Hunt et al. 1988; Zilitinkevich et al. 2006). The vertically inhomogeneous and anisotropic statistical structure for horizontal and vertical components is determined by the blocking of eddies, either by the sea/land surface (Hunt 1984) if there is no significant shear (outer part of tropical cyclone) or by the mean velocity gradient in the jet (near the eyewall). At this level the length scale $L_x^w \propto \sigma_w / dU/dz$ (where $U$ is the mean azimuthal speed, $z$ is the height, $\sigma_w$ is the standard deviation of vertical fluctuating wind speed) is reduced by the local mean shear and by the stable mean gradient of the potential temperature, because typically in the stable boundary layer the buoyancy frequency ($N = \left[ g(d\bar{\theta}/dz)T_0^{-1} \right]^{1/2}$, where $g$ is the local acceleration of gravity, $\bar{\theta}$ is mean potential temperature, $T_0$ is the ground-level temperature) can be of the same order as $dU/dz$ (Hunt et al. 1985) |
| $z \approx z_{max}$ | The effects of the positive radial gradient of turbulence near the eyewall, i.e. $d\sigma_V^2/dr > 0$, leads to a mean outward radial velocity ($V > 0$) near the surface in the lower part of the boundary layer, driven by Reynolds stresses (Townsend 1976). Note that where $r \geq R_{ew}$, since $dV/dr > 0$, by continuity a mean downward flow outside and inside of the eyewall was observed. By interaction with the mean shear $dU/dz$ this contributes to a local increase in the swirl velocity (proportional to $-\overline{W}dU/dz$, where $\overline{W}$ is the mean vertical velocity). Farther from the eyewall, however, where $r \approx h$, the mean radial flow reverses and an inward mean velocity is generated by the mean radial pressure gradient produced by the swirl. The mean flow is also affected by the strong convective turbulence changing the vertical gradient of the turbulent shear stress (i.e. $d\tau/dz > 0$, where $\tau$ is the shear stress) that amplifies the jet flow in the lower boundary layer (Owinoh et al. 2005). Thus in the lower part of the convective layer, where $z \approx z_{max}$, either the mean azimuthal velocity $U$ reaches a single maximum with peak value $U_{max}$, (where $dU/dz = 0$), or a secondary maximum occurs depending on these two processes. As explained above, in these shear regions with weak convection, roll structures are generated, as occurs in slightly unstable boundary layers over level surfaces (Smedman et al. 2007). The existence of the maxima in the mean velocity profiles tends to separate the eddy structures above and below the levels where there is a maximum in the mean velocity, i.e. low-level jets (Smedman et al. 2004) |
| $z_{LLJ} < z < z_{max}$ | If this intermediate layer exists, the turbulence is largely driven by the mean wind shear $dU/dz$ |
| $z = z_{LLJ}$ | In some situations, the mean azimuthal velocity $U$ has a local maximum at $z = z_{LLJ}$ associated with a low-level jet |
| $l_s < z < z_{LLJ}$ | In the atmospheric surface layer (ASL), except within the eyewall, the turbulence is largely shear dominated and not significantly affected by surface processes or roughness elements (e.g. spray layer, which may have some effects as explained below, surface waves or surface obstacles). In this eddy surface layer there is a wide range of eddy scales. Here top-down convective and sheared eddies, generated at or above the level of the velocity maximum, extend down to the level $z$ where shear dominates their structure (Townsend 1976; Perry and Abell 1977). Their horizontal length scales are larger than $z$, but the scales of the vertical fluctuations are reduced by blocking at the surface (Hunt and Carlotti 2001; Högström et al. 2002) |

**Table 1** continued

| Levels | Turbulence dynamics |
|---|---|
| $z \approx l_s$ | As the tropical cyclone moves over the ocean, water droplets are generated by breaking waves and the fluctuating turbulent drag at the surface (Komori et al. 2010), which is proportional to the friction velocity $u_*$. The surface-generated eddies grow in size as they move upwards at an average velocity of order $u_*$, and transport the smallest droplets within them (Hunt et al. 2007). For the droplets that break up at a height $z$ with critical radius $a'(z)$ the surface tension force $\gamma a'$ (where $\gamma$ is the surface tension of the droplets) is less than the drag force breaking up the droplets by the inertial sub-range eddies determined by the dissipation rate $\varepsilon \approx u_*^3 z^{-1}$, so that $a'(z) \approx (\gamma/\rho)^{3/5}/\varepsilon^{2/5}$ (where $\rho$ is the air density). By considering how such droplets are trapped where their fall speed $(a'g)^{1/2}$ is of the same order as the eddy velocity, it follows that the typical height where small-scale droplets are suspended is of order $l_s \approx u_*^8 / \left[ g^5 (\gamma/\rho)^3 \right]^{1/2}$. When $u_* \geq 0.2$ m s$^{-1}$, as in the eyewall region, $l_s$ is significantly greater than the simple Charnock trajectory height $\alpha_c u_*^2 g^{-1}$ (where $\alpha_c$ is the Charnock's constant (Charnock 1955))—just as suspended dust particles rise higher than saltating particles on a dusty surface (Nalpanis et al. 1993). As the droplets evaporate, they release heat on the scale $l_s$ of the surface eddies and thence generate a significant buoyancy flux in the rising warm eddies on scale $l_{sd}$ (Lighthill 1998; Barenblatt et al. 2005). As in the convective boundary layer, thermal plumes develop that first grow in scale as they rise and then are distorted in the surface shear layer. Surface-layer turbulence then transfers their energy over larger scales in the spectrum and also to greater heights. When $u_*$ is smaller, and $l_s$ corresponds to the Charnock estimate, then eddy shearing enhanced by the mean shear dominates the near-surface turbulence. This increase in small-scale energy near the surface is analogous to that in a turbulent boundary layer over a roughness change near a coastline, e.g. Panofsky et al. (1982) |
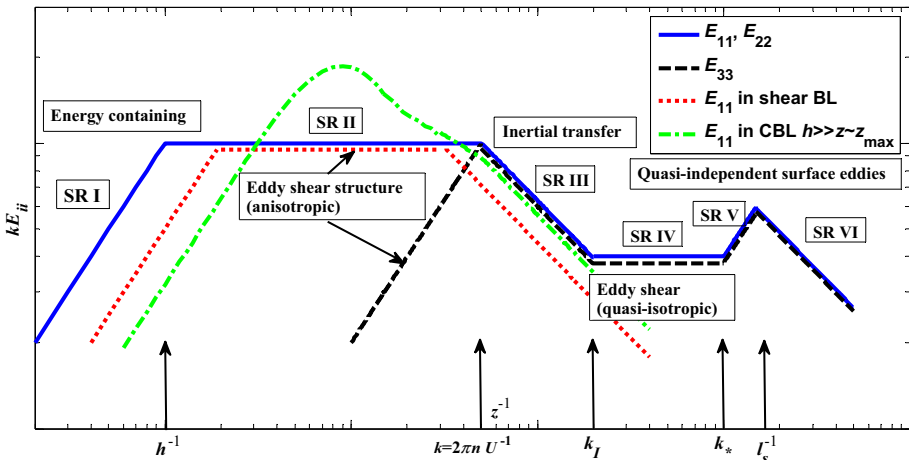


**Fig. 2** Schematic diagram of the sub-ranges (SR) of the turbulent velocity spectra in the tropical cyclone boundary layer. Note the quasi-independent small-scale spectra associated with intense eddy motions in the surface layer (e.g. waves and coastal roughness change). For the sake of comparison, the longitudinal spectra $E_{11}$ (*dot-dashed green line*) in the convective boundary layer (Hunt 1984) and $E_{11}$ (*red dot line*) in the surface layer of a neutral boundary layer (Hunt and Morrison 2000) are presented. Note that $k_I^{-1}$ and $l_s$ are much smaller in the outer-vortex region of the tropical cyclone

We focus on the sub-ranges of the spectra for the longitudinal and lateral components of turbulence near the eyewall (i.e. $r \approx R_{ew}$) in the eddy surface layer where $l_s < z < z_{LLJ}$ (This analysis is based on the measurements at 10 m, see Sect. 4.2).

(1) In sub-range I ($k < h^{-1}$), turbulent energy is produced by buoyancy and shear, and the one-dimensional energy spectrum does not vary with $k$ (Townsend 1976; Hunt 1984),

$$E_{11} \propto E_{22} \propto u_*^2 h \tag{1}$$

where $E_{11}$ and $E_{22}$ are the longitudinal and lateral energy spectra, respectively.

(2) Sub-range II is the range ($h^{-1} < k < z^{-1}$, or $h^{-1} < k < z_{LLJ}^{-1}$ if there is a local maximum—low-level jet in the mean velocity profile) where the main mechanism is the formation of elongated sheared eddy structures (Hunt and Carruthers 1990; Lee et al. 1990). Scaling allows for the blocking of the eddies by the ground and, if it is significant, by the shear of the jet (Townsend 1976; Hunt and Morrison 2000; Hunt and Carlotti 2001). The eddies in this sub-range have a self-similar spectrum for longitudinal and lateral components,

$$E_{11} \propto E_{22} \propto u_*^2 k^{-1} \tag{2}$$

and the blocking effect reduces the vertical component,

$$E_{33} \propto u_*^2 z \tag{3}$$

where $E_{33}$ is the vertical energy spectrum.

The streaky structure of the horizontal fluctuations in this layer is generally associated with roll structures of longitudinal vorticity, especially with rough surface conditions, e.g. at coastlines or over large waves (Wurman and Winslow 1998). Commonly observed streaky tree damage patterns are consistent with these roll structures (see Fitzroy 1863).

(3) In sub-range III ($z^{-1} < k < k_I$ or $z_{LLJ}^{-1} < k < k_I$, where $k_I$ is the transition wavenumber between sub-ranges III and IV), the eddy motions are quasi-homogeneous because they are smaller than the distance, $z$, to the ground. They are determined by the self-similar inertial sub-range dynamics with a net transfer of energy $\varepsilon \approx u_*^3 z^{-1}$ towards a further range of smaller scales, so that

$$E_{ii} \propto \left(u_*^3/z\right)^{2/3} k^{-5/3} \tag{4a}$$

where $E_{ii}$ could be $E_{11}$, $E_{22}$ and $E_{33}$ for the longitudinal, lateral and vertical components, respectively.

The self-similarity of the eddy structure in this range as $k$ and $z$ vary is demonstrated by rewriting Eq. 4a as

$$k E_{ii} \propto u_*^2 (kz)^{-2/3} \tag{4b}$$

Interactions with smaller eddies with wavenumber $k > k_I$ determine the upper limit of this sub-range.

Near the surface in the boundary layer of tropical cyclones, dynamically active and passive near-surface processes lead to ranges of small quasi-independent eddies characterized by sub-ranges IV, V and VI. The characteristic length scale of the most energetic sub-range approximates $l_s$.

The dynamically active surface convective motions, with root-mean-square velocity $w_*^s$, driven by the relative movement of the spray droplets (Elghobashi and Truesdell 1993; Ferrante and Elghobashi 2003) and by evaporation of spray droplets (Lighthill 1998), add extra energy at the length scale $l_s$ of the vertical profile of the droplet distribution, as explained in Table 1. The mean drag associated with these droplet motions also induces additional turbulence, with length scale greater than $l_s$. The mean vertical gradient of this turbulent layer produces an additional surface shear stress $u_*^s$. The energy of the

independently generated near-surface fluctuations, denoted by $u_s'^2$, is the sum of these components given by

$$u_s'^2 = u_*^{s2} + w_*^{s2} \tag{5}$$

noting that both these components contribute to the spectra $E_{ii}$.

Since the contributions of these near-surface processes increase with the square of the mean wind speed, they are much stronger near the eyewall, and to decrease rapidly with height above the surface $z$. The matching sub-ranges in this near-surface region have different dynamics and forms.

(4) Sub-range IV ($k_I < k < k_*$, where $k_*$ is the transition wavenumber between sub-ranges IV and V) is the range between the larger scale, shear-driven inertial sub-range spectra $k < k_I$ and the near-surface processes determined by $u_s'^2$, which as Elghobashi and Truesdell (1993) demonstrated lead to up-scale transport. The transition sub-range beyond the inertial sub-range in Eq. 4b (which depends on the height $z$), is determined by highly sheared eddies that are smaller than the distance to the ground or sea surface and therefore are quasi-homogeneous and isotropic, unlike the range of sheared eddies in sub-range II. The transition sub-range is determined by the additional surface shear stress $u_*^s$, whence by dimensional scaling

$$E_{ii} \propto u_*^{s2} k^{-1} \tag{6}$$

Note that this kind of spectrum for a sheared quasi-homogeneous turbulence was measured by Kader and Yaglom (1991), and derived theoretically for time-dependent rapid distorted turbulence (Hanazaki and Hunt 2004).

By matching the energy transfer in the sub-ranges III and IV, it follows that the energy of small-scale eddies is related to $u_*$, $z$ and $k_I$,

$$u_*^{s2} = u_*^2 (k_I z)^{-2/3} \tag{7}$$

(5) Sub-range V ($k_* < k < l_s^{-1}$) has contributions from the large scales related to near-surface processes, where

$$E_{ii} \propto u_s'^2 l_s \tag{8}$$

By matching sub-ranges IV with V at $k = k_*$, it follows that near $R_{ew}$ for $z < z_{max}$, the transition wavenumber of the spectrum between these two sub-ranges is given by $u_*^{s2} k_*^{-1} = u_s'^2 l_s$,

$$k_* = \left( u_*^s / u_s' \right)^2 l_s^{-1} \tag{9}$$

(6) Sub-range VI ($l_s^{-1} < k \ll \eta^{-1}$, where $\eta$ is the Kolmogorov microscale, which is of the order of mm as verified by hot-wire measurements in turbulent boundary-layer field experiments, (Kaimal and Finnigan 1992) is determined by the approximately independent near-surface eddies that are smaller than $l_s$, so that,

$$E_{ii} \propto \left( u_s'^3 / z \right)^{2/3} k^{-5/3} \tag{10}$$

Note that the quasi independence of the different eddy structures in the separate sub-ranges partly results from the shielding by the thin shear-layer structure of the microscale eddies (Hunt et al. 2014; Ishihara et al. 2013). For the spectra of turbulence in higher level of the boundary layer ($z_{LLJ} < z < h$), the vertical structure of the airflow and temperature, especially the spectrum of the vertical wind component, are affected significantly on scales of order $z_{LLJ}$ by the variation in the mean shear at $z_{LLJ}$ and by shear and stratification at

the top of the PBL. The characteristic sub-ranges and the relative effects are quite sensitive to these mean gradients—as seen in the data presented in Sect. 4.2. The main change is the absence of strong shear so that sub-range II does not exist.

In the outer regions of the tropical cyclone, where $r \approx R_{ov}$, the mean radial motions are not significant and the turbulence dynamics in the lower layers of the tropical cyclone is similar to that of the atmospheric boundary layer with strong convection (i.e. $h/L_{mo}$ ranges from about $-10$ to $-1$ where $L_{mo}$ is the Obukhov length). In this boundary-layer region there are strong vertical thermal plumes and weaker shearing motions (Zilitinkevich et al. 2005).

From many field studies of the spectra of convective turbulence and theoretical models (e.g. Hunt 1984), and from considering the energy from independent small-scale surface-layer processes (Hunt 2000), it is hypothesized that the sub-ranges of the spectra for the outer-vortex regions ($l_s < z < h$ and $r \approx R_{ov}$) of tropical cyclones within the boundary layer have the following forms,

(1) in sub-range I ($k < h^{-1}$)

$$E_{ii} \propto w_*^2 h \tag{11}$$

where $w_*$ is the friction velocity in the outer-vortex regions of tropical cyclones.

(2) in sub-range II ($h^{-1} < k < z^{-1}$)

$$E_{11} \propto E_{22} \propto w_*^2 k^{-1} \tag{12}$$

$$E_{33} \propto \left(w_*^3/h\right)^{2/3} z^{5/3} \tag{13}$$

(3) in sub-range III ($z^{-1} < k < l_s^{-1}$), inertial sub-range convective eddies

$$E_{ii} \propto \left(w_*^3/h\right)^{2/3} k^{-5/3} \tag{14}$$

(4) sub-range IV, which is dominated by additional shearing associated with droplets, has a similar form as in the eyewall region ($r \approx R_{ew}$). Note that in this sub-range the eddies are quasi-homogeneous and isotropic, and determined by $u_*^s$.

(5) sub-ranges V and VI are not significant in the outer-vortex region where $w_* \ll u_*$, thus $l_s \approx u_*^8/\left[g^5(\gamma/\rho)^3\right]^{1/2}$ decreases and the processes associated with droplets are confined to the Charnock distance $\alpha_c w_*^2 g^{-1}$. Note that the low-level jet may still exist in the outer vortex regions associated with interaction between the buoyant convection and the mean swirl (Owinoh et al. 2005).

## 3 Coastal Wind Experiments on the Tropical Cyclone Boundary Layer

### 3.1 Observation Towers and Instrumentations

The measurements reported in this study were taken in tropical cyclone Nuri from a 60-m high observation tower located on Delta Island on the south China coast and in tropical cyclone Hagupit from a 100-m high observation tower located on Zhizai Island. The data are compared with the spectral sub-ranges analyzed in the previous section. An earlier experimental study has been conducted to establish a data-driven model for velocity spectra in tropical cyclone winds using data obtained at Zhizai Island in tropical cyclone Hagupit (Li et al. 2012).

Delta Island is located at the entrance of the Pearl River estuary, and is fairly exposed to flow over open waters from the northern direction, with Qingzhou Island about 2.5 km distant. Datouzhou Island is located about 4.5 km to the south and Guishan Island and Macau
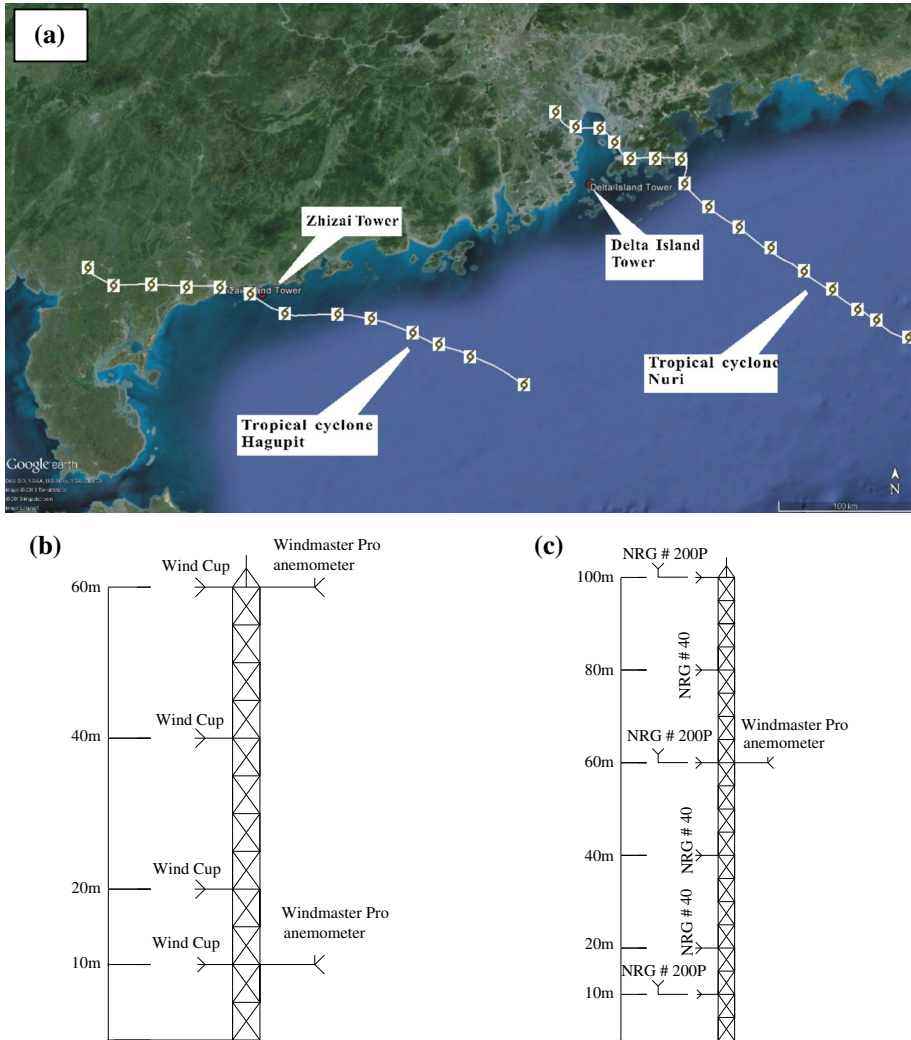
**Fig. 3** Full-scale measurement details: **a** track of tropical cyclones Nuri and Hagupit and the location of Delta Island tower and Zhizai tower; **b** layout of instruments on Delta Island Tower; and **c** layout of instruments on Zhizai Tower

city are more than 10 km to the east and west, respectively. The geographical coordinates of the tower are 113°42′34.5″ E longitude and 22°08′28.6″ N latitude, while the base elevation of the Delta tower is 93 m. The diameter of the island is about 2 km and the peak slope of the terrain on the island is about 0.1. Although the form of wind spectra can change in accelerating flows (Britter et al. 1979), in this case the flow distortion over these low hills is small.

Figure 3a shows the exposure of the Delta Island tower and the track of tropical cyclone Nuri. The shortest distance from the Delta Island tower to the centre of tropical cyclone Nuri was about 34 km. Therefore, the radial position, $r$, of the tower is within a distance of 1.5 $R_{ew}$, where $R_{ew}$ is the radius of the eyewall. Four levels of sensors were installed on the

tower at elevations of 10-, 20-, 40- and 60-m. The data acquisition system measures the three wind components at 10- and 60-m heights using sonic anemometers (WindMaster$^{TM}$ Pro 3D, Gill Instruments Limited) with a sampling frequency of 10 Hz. Four cup anemometers (NRG #40C, NRG systems, Inc.) were installed at 10-, 20-, 40- and 60-m heights to collect wind-profile data; data from the four cup anemometers (NRG #40C, NRG systems, Inc.) include 1-h mean wind speeds and directions at each 1-h interval. The layout of instrument locations on the Delta Island tower is shown in Fig. 3b.

Zhizai Island, where measurements in tropical cyclone Hagupit were taken, is a small island with a length of about 120 m, width of about 50 m, and the highest location above sea level is about 11 m. The geographical coordinates of the tower are 111°22′47.30″E longitude and 21°27′04.12″N latitude. The shortest distance from Zhizai tower to the mainland is about 4.5 km. Dazhuzhou Island is located on the south side of Zhizai Island at a distance of 1 km. The Zhizai location is fairly well exposed to open waters in the north-west to north-north-east directions and the sea exposure in the east-north-east to east-south-east directions. The tower is equipped with seven levels of sensors at 8-, 10-, 20-, 40-, 60-, 80- and 100-m heights. The data acquisition system measured the three wind components at the 60-m height using sonic anemometer (WindMaster$^{TM}$ Pro 3D, Gill Instruments Limited) with a sampling frequency of 10 Hz. Six cup anemometers (NRG #40C, NRG systems, Inc.) were installed at 10-, 20-, 40-, 60-, 80- and 100-m heights to collect wind-profile data and three wind direction vanes (NRG #200P, NRG systems, Inc.) were located at 10-, 60- and 100-m heights to collect wind direction data. The outputs from the cup anemometers and vanes are the 10-min mean wind speeds and directions recorded at 10-min intervals, respectively. A temperature sensor (NRG #110s, NRG systems, Inc.) and a barometer (NRG BP20, NRG systems, Inc.) were installed at 8-m height. The shortest straight line from the Zhizai Tower to the centre of tropical cyclone Hagupit is about 8.5 km, i.e. less than the radial distance to the eyewall. The layout of instrument locations on the Zhizai tower is shown in Fig. 3c.

3.2 The Data

The original anemometer data were pre-processed following the quality-control procedures illustrated in Li et al. (2012). The variations of the mean velocities for tropical cyclones Nuri and Hagupit are presented in Fig. 4a and b, where the typical structures can be observed, i.e. very low wind speeds within the eye (with radius of about 10–20 km), peak velocities and sharp gradients near the eyewall, and mean wind speeds decreasing in the outer-vortex regions.

Figure 4a presents the 10-min mean wind speed and direction of tropical cyclone Nuri at 10- and 60-m heights during the period of August 22–23, 2008. The maximum mean wind speeds were 29 and 33 m s$^{-1}$ at 10- and 60-m heights, respectively. Sets of data for a 1-h period were selected in four regions of the tropical cyclone wind field to analyze the spectral characteristics of tropical cyclone winds in the eddy surface layer and in the surface layer. In particular, four datasets were extracted in correspondence of the front-side outer-vortex region (FOV), front-side eyewall region (FEW), back-side eyewall region (BEW) and back-side outer-vortex region (BOV), as shown in Fig. 4a. Table 2 lists the wind characteristics of the four 1-h datasets.

Figure 4b presents the 10-min mean wind speed and direction of tropical cyclone Hagupit during the period of September 24–25, 2008 at 60-m height. In the interval between 0900 and 1120 local time (UTC +8) too many spikes were observed in the measurements, so these datasets were discarded. The maximum mean wind speeds before and after the passage of the tropical cyclone eye were 46 and 40 m s$^{-1}$, respectively. The observed maximum 3-s gust
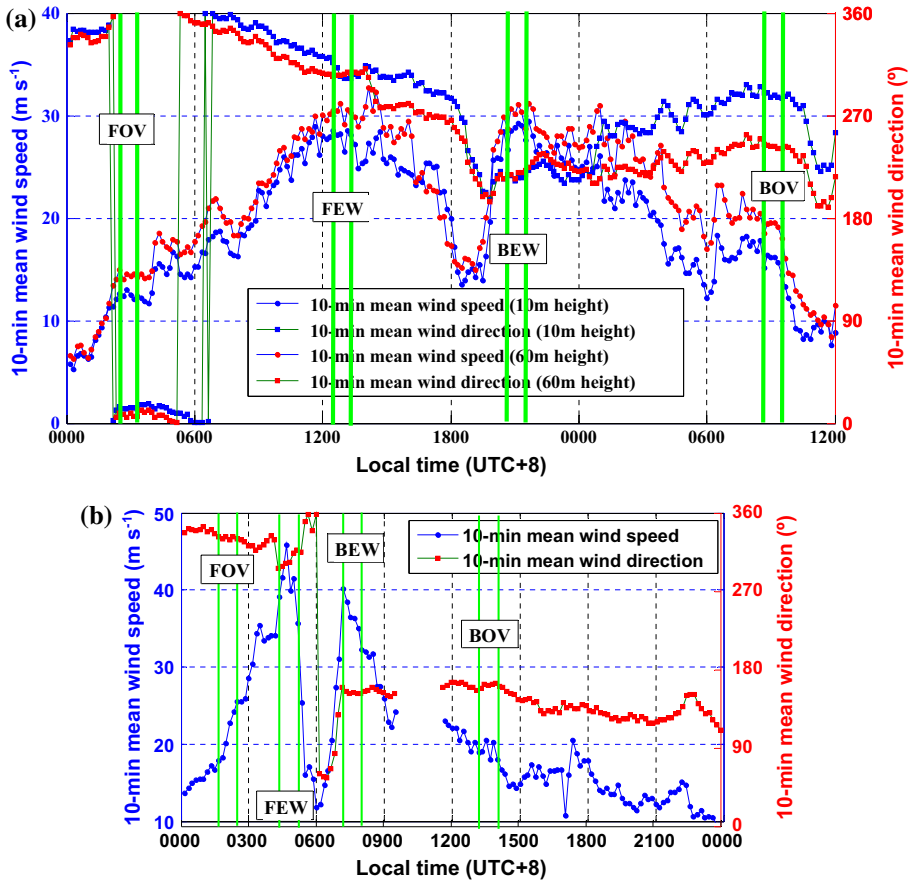
**Fig. 4** Time history of the 10-min mean wind speed and direction in tropical cyclones: **a** tropical cyclone Nuri; and **b** tropical cyclone Hagupit. (FOV denotes the front-side outer-vortex region, FEW denotes the front-side eyewall region, BEW denotes the back-side eyewall region and BOV denotes the back-side outer-vortex region)

wind speed was 57 and 49 m s$^{-1}$ before and after the passage of the tropical cyclone eye, respectively. Analogous to what was done for tropical cyclone Nuri, sets of 1-h data were selected in the four regions FOV, FEW, BEW and BOV, and their statistical characteristics are also reported in Table 2.

## 4 Measurements and Comparisons with Theoretical Spectral Models

### 4.1 Mean Velocity Profiles

Figure 5a presents the mean wind-speed profiles at the Delta Island tower for the tropical cyclone Nuri. As the cup anemometers give the 1-h mean wind speeds, the wind profiles for the four regions (FOV, FEW, BEW and BOV) are given by the average value for two hours of data around the selected time windows shown in Fig. 4a. The mean profiles of the wind speeds at the Zhizai tower are presented in Fig. 5b for the tropical cyclone Hagupit. In

**Table 2** Statistical characteristics of selected data for tropical cyclones Nuri and Hagupit

| Tropical cyclone | Height (m) | $U$ (m s$^{-1}$) | $u_*$ (m s$^{-1}$) | $H_0$ (W m$^{-2}$) | $z/L_{mo}$ | $I_u$ | $I_v$ | $I_w$ | $\beta$ | $T$ (K) |
|---|---|---|---|---|---|---|---|---|---|---|
| *Nuri* | | | | | | | | | | |
| FOV | 10 | 13 | 0.21 | −0.01 | 0.10 | 0.15 | 0.11 | 0.06 | 8.73 | 307 |
| | 60 | 14 | 0.27 | −0.01 | 0.10 | 0.05 | 0.04 | 0.02 | 2.49 | 309 |
| FEW | 10 | 28 | 0.97 | 0.00 | 0.00 | 0.11 | 0.09 | 0.05 | 3.14 | 306 |
| | 60 | 30 | 0.67 | −0.05 | 0.11 | 0.07 | 0.05 | 0.04 | 3.26 | 309 |
| BEW | 10 | 28 | 0.90 | −0.17 | 0.03 | 0.11 | 0.07 | 0.04 | 3.45 | 304 |
| | 60 | 30 | 0.57 | 0.16 | −0.57 | 0.08 | 0.05 | 0.04 | 4.24 | 307 |
| BOV | 10 | 16 | 0.46 | 0.01 | −0.01 | 0.11 | 0.07 | 0.04 | 3.75 | 298 |
| | 60 | 19 | 0.58 | 0.03 | −0.09 | 0.07 | 0.05 | 0.03 | 2.16 | 302 |
| *Hagupit* | | | | | | | | | | |
| FOV | 60 | 21 | 0.45 | −0.03 | 0.27 | 0.10 | 0.09 | 0.05 | 4.75 | 305 |
| FEW | 60 | 41 | 1.05 | −0.04 | 0.03 | 0.13 | 0.10 | 0.05 | 4.87 | 303 |
| BEW | 60 | 36 | 0.54 | −0.10 | 0.52 | 0.10 | 0.09 | 0.04 | 6.44 | 303 |
| BOV | 60 | 19 | 0.71 | −0.05 | 0.12 | 0.10 | 0.07 | 0.04 | 2.81 | 302 |

$U$ is the 10-min mean wind speed, $u_*$ is the friction velocity, $H_0$ is the heat flux, $z/L_{mo}$ is the atmospheric stability parameter, $L_{mo}$ is the Obukhov length scale, computed with local flux values. $I_u$, $I_v$ and $I_w$ are the turbulence intensities for the longitudinal, lateral and vertical components, respectively; these are defined as the ratio of standard deviation $\sigma$ of the corresponding component to mean wind speed $U$; $\beta$ is the ratio of the standard deviation $\sigma_u$ of the longitudinal component to the friction velocity $u_*$; $T$ is the mean temperature at the corresponding height

this case, the datasets used to plot the wind-speed profiles are taken exactly within the same time window shown in Fig. 4b, i.e. the wind profiles are obtained as the average value of six 10-min length datasets.

Figure 5 and Table 2 show that, even though the mean profiles and the turbulence structure differ from one tropical cyclone to another, they show some common features. In both cases, a shear layer is apparent from the 10-m height to about the 40-m height in the eyewall regions (FEW and BEW) with a local maximum velocity at $z \approx z_{LLJ}$. It should be observed that, due to the limited number of anemometers installed along the towers, the accurate height of the low-level jet ($z_{LLJ}$) could not be precisely captured, but it was estimated in the range between the 20- and 60-m heights in the eyewall regions. In the outer-vortex regions, the low-level jet was less pronounced. The wind-speed profiles follow the typical logarithmic law below $z_{LLJ}$ and the height of this shear layer is consistent with the length scale of wind spectra in the eyewall regions. The vertical velocity profile observed by the mini-sodar at Siu Ho Wan in Hong Kong by the Hong Kong Observatory in tropical cyclone Nuri also exhibited strong subsidence from 100- to 40-m heights (Wong and Chan 2010). This observation is quite consistent with the horizontal component profile in Fig. 5a and the flow structure shown in Fig. 1b. The formation of a jet by strengthening convection in the eyewall region as it moves is consistent with the theoretical model of Owinoh et al. (2005).

In the outer-vortex regions (FOV and BOV) the height of the local maximum wind speed increases, and there is no significant shear layer, especially in tropical cyclone Hagupit, which is also reflected in the wind spectra in these regions. From the Hagupit data in Fig. 5 and Table 2, it can be seen that the scale of energy-containing eddies ($\sigma_w/dU/dz$) is of the order of about 30 m (Hunt et al. 1985).
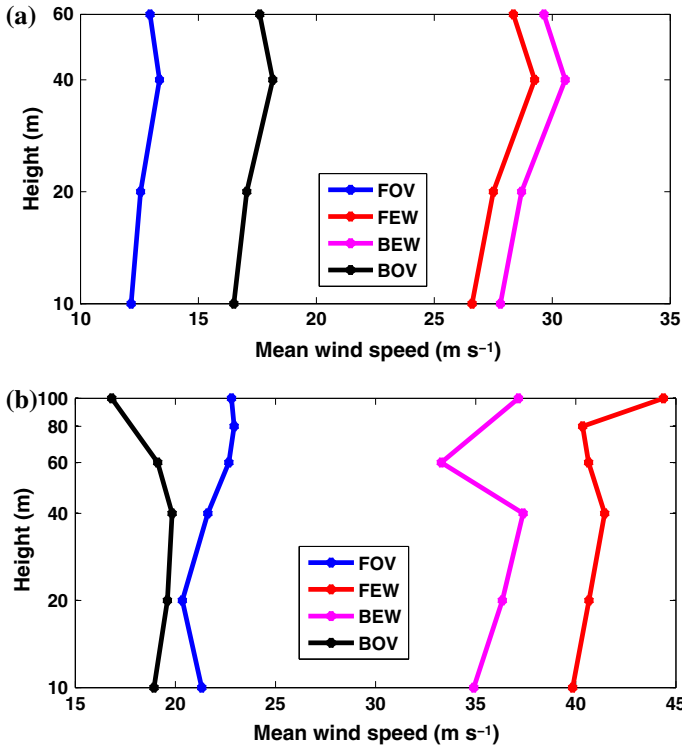
**Fig. 5** Mean wind speed profiles at the different radial positions (defined in Fig. 4): **a** tropical cyclone Nuri; and **b** tropical cyclone Hagupit. Note the low-level jet can be clearly seen for the regions near the eyewall (FEW and BEW), while it is less pronounced in the outer regions (FOV and BOV)

## 4.2 Velocity Spectra of Tropical Cyclone Winds in the Eddy Surface Layer and in the Surface Layer

Figure 6 shows the longitudinal wind velocity spectra in tropical cyclone Nuri at 10- and 60-m heights, which are at a level within and above the eddy surface layer. The measured spectra are based on 1-h long datasets in the corresponding region. The spectra are represented in terms of the non-dimensional frequency $f = nz/U$ (where $n$ is the natural frequency, $z$ is the height, $U$ is the mean azimuthal speed), with corresponding wavenumber $k = 2\pi f/z$ and wavelength $\lambda = U/n$. The spectra are normalized by the variance of the corresponding components. The figure clearly shows the existence of spectral characteristic sub-ranges, and how they change with height, radius, and between the forward and backward regions. Note that the fact that the measurement location is 93 m above sea level can have some effect on the estimated turbulence; these effects, however, can be considered minimal (e.g. Britter et al. 1979). In the following, some observations are summarized.

In sub-range I the length scales exceed 3,000 m near the eyewall as a result of the elongated shear structures (typically rolls), which can be greater than the depth of the boundary layer, as with the PBL over flat surfaces (Högström et al. 2002).

For the eddy scales less than about 3,000 m to about 10 m (or $z_{LLJ}$ if the low-level jet exists) in sub-range II (at the observing level of 10 m), there is a distribution of sheared structures that are in contact with the surface since $kz < 1$ (Hunt and Morrison 2000; Högström et al.

2002). Sub-range II, however, does not exist for the observations taken at higher levels in the surface layer, where there is no significant shear and eddy scales are $< z$.

Sub-range III is a 'short' inertial sub-range with even smaller length scales for observations at 10-m height, since $kz > 1$. For observations at 60-m height, however, where $kz > 1$, the inertial sub-range is wider, especially for the front-side eyewall (FEW) regions than for the back-side eyewall (BEW) regions where the advected eddies from the eyewall region affect the spectra. In tropical cyclone Nuri with the low-level jet in the near surface layer, sub-range III extends from about 3,000 m down to $z_{LLJ}$. The very large-scale eddies are generated in the upper-layer convection where $z > h$.

Sub-range IV is characterized by length scales less than the order of $z_{LLJ}$ and is affected by strong shear and surface processes. Note that the transition wavenumber $k_I$ is smaller, where $z$ is larger, as explained in Sect. 2.

Considering the sub-ranges IV and V, it should be noted that the total energy of the independent small scales influenced by surface processes are larger for the backward (B) facing flow regions as compared with the forward (F) facing flow regions. This is probably due to the fact that there is more time for surface processes to influence the turbulence at the measurement height in the case of B regions.

For the outer-vortex regions (FOV and BOV), where the surface shear at the height of the instrument is still significant but less marked, the spectra in the characteristic ranges are similar for sub-ranges I and II. But for the front-side outer-vortex (FOV) region, the inertial sub-range (sub-range III) is more pronounced for the upwind spectra (as explained above) and sub-range IV is less marked. For the back-side outer-vortex (BOV) region, the small-scale downwind effects and surface-layer turbulence contributions are more pronounced, which results in a less pronounced inertial sub-range.

The spectra of the fluctuating velocity components (longitudinal, lateral and vertical, indicated as $u$, $v$ and $w$, respectively) at a height of 60 m for the tropical cyclone Hagupit were also analyzed (see Table 2). The spectra are normalized on the standard deviation $\sigma_u$, $\sigma_v$, $\sigma_w$ or $\sigma_\theta$. The characteristic sub-ranges are compared with the conceptual model discussed in Sect. 2 and shown in Fig. 2. As can be seen from the mean profile in Fig. 5b, the measurement height $> z_{LLJ}$ and is therefore in the ASL. Based on what was previously observed, the convective turbulence gives a significant contribution to the formation of a low-level jet. Also, a spectral description of temperature data, $S_\theta$, is provided to illustrate how the energy is distributed in comparison to velocity fluctuations. By observing the spectra of fluctuating velocity components and fluctuating temperature presented in Figs. 7 and 8, the following observations can be made.

Sub-range I, which extends over horizontal velocity and temperature scales greater than about 500 m, shows the effects of large-scale convective turbulence in the tropical cyclone both near the eyewall and in the outer-vortex region. Note that the greater amplitude of the large-scale fluctuations near the eyewall are likely to be affected by the irregular shape and random movements of the eyewall.

In sub-range II, the non-uniform shear in the ASL has only a weak effect on the longitudinal and lateral velocity spectra, $S_u$ and $S_v$, by straining or blocking. This observation is different from the effects on the vertical velocity and the temperature spectra. For $S_u$ and $S_v$, there is no characteristic sub-range II. The weak shear (near the eyewall), however, leads to a characteristic sub-range where frequency weighted vertical velocity spectrum $nS_w$ and temperature spectrum $nS_\theta$ are approximately constant over length scales between about 40 m ($f = nz/U \approx 1.5$) and 1,000 m ($f = nz/U \approx 0.06$). Note that the vertical velocity spectrum $nS_w$ and the temperature spectrum $nS_\theta$ do not show the sub-range II in the outer-vortex regions.
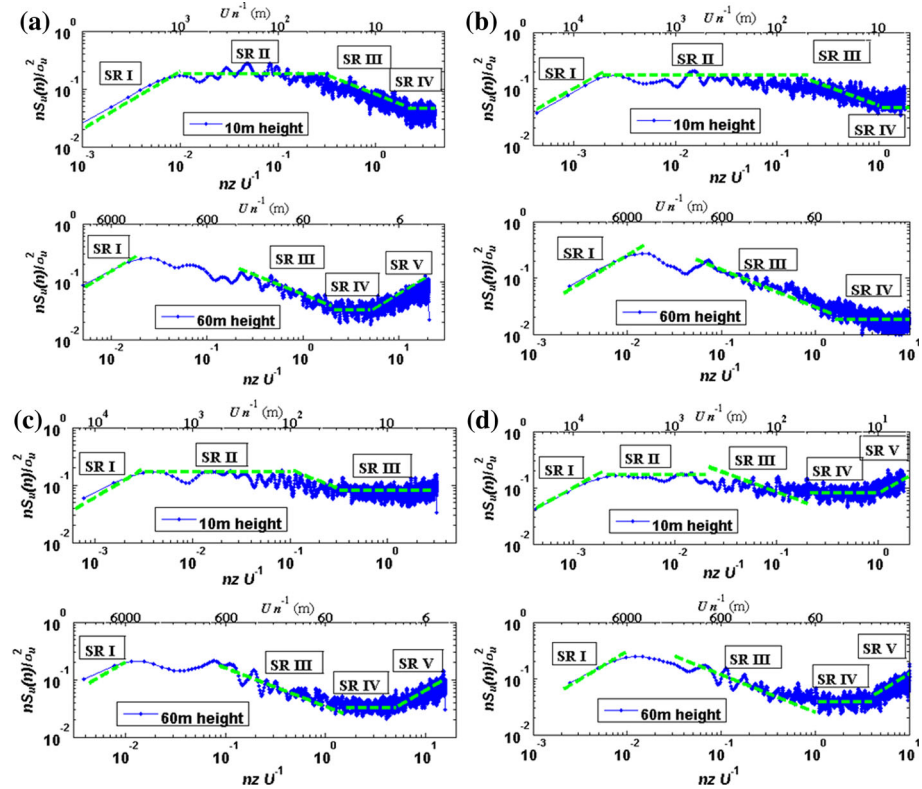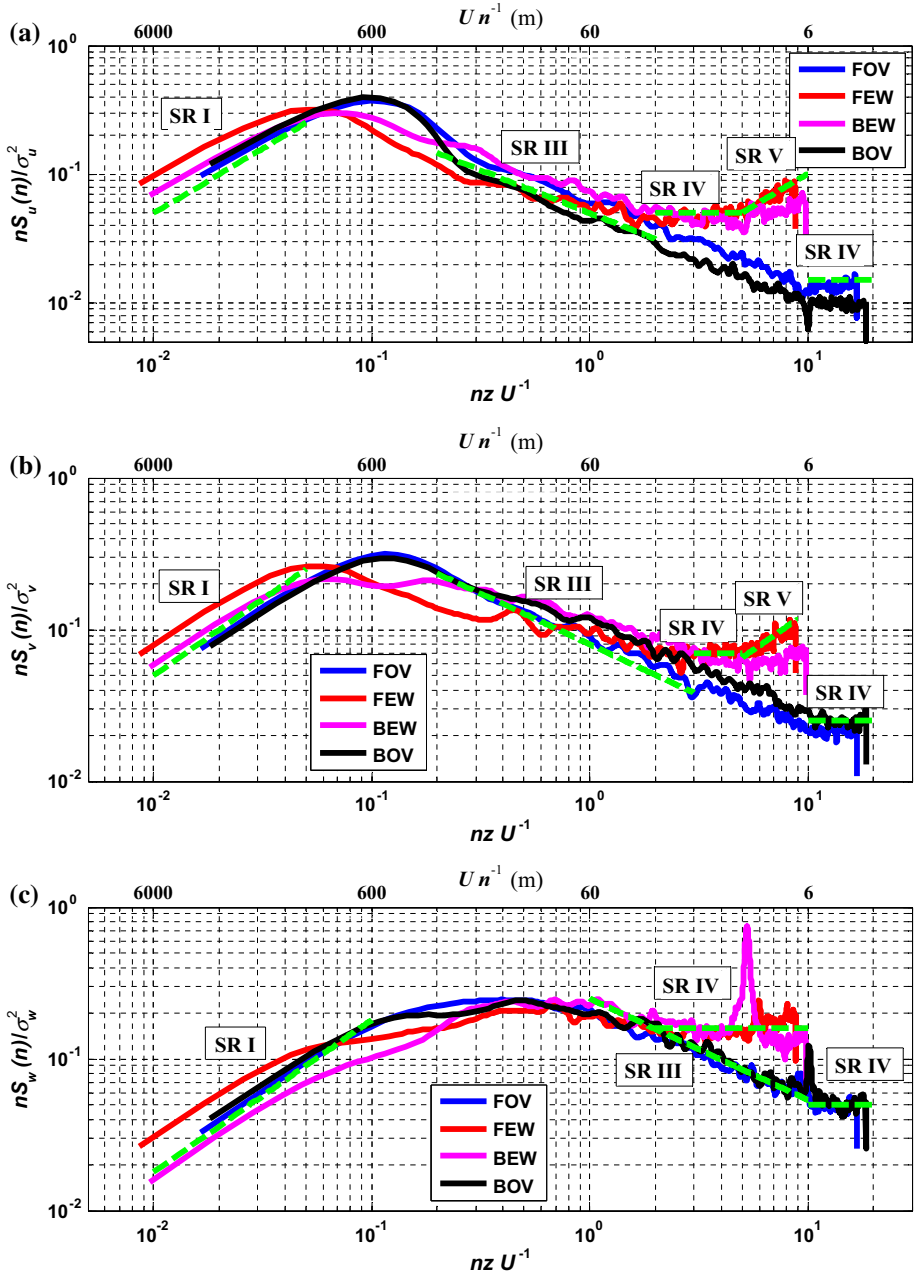
**Fig. 6** Longitudinal wind-speed spectra for tropical cyclone Nuri (*dash lines* correspond to conceptual model of Sect. 2 and Fig. 2, and the *dot lines* are the measured spectra): **a** front-side outer-vortex region (FOV); **b** front-side eyewall region (FEW); **c** back-side outer-vortex region (BOV); and **d** back-side eyewall region (BEW)

The extent of the inertial sub-range spectra (sub-range III) is limited in the eyewall region by the shear; this occurs for larger scales in the $S_u$ and $S_v$ spectra, and for smaller scales in the $S_w$ and $S_\theta$ spectra. In the outer-vortex regions, where the measurement height is in the ASL, however, this sub-range extends from 500 m down to about 10 m. In the spectra of the temperature fluctuations there are wider inertial sub-ranges and the eddy scales extend from about 600 m down to 10 m in the front-side outer-vortex (FOV) sector in the airflow approaching the tropical cyclone. This may be due to temperature difference between the air and sea, which is greater than in the case of the well-mixed airflow in the back-side outer-vortex (BOV) sector downwind of the tropical cyclone.

For sub-ranges IV and V within and near the eyewall (at locations defined in Fig. 5b), Figs. 7 and 8 show that small-scale eddies with length scales less than about 40 m are generated in the surface layer. The spectral energy (at a given wavenumber) is about 3–10 times more intense than that in the inertial sub-range for convective or shear boundary layers. This is associated with the transition in the eyewall layer between complex convection and sheared eddies produced by the low-level jet. Note that the eyewall eddy motions (with spectral sub-ranges IV and V) are quite separate from the roll structures in the eddy surface layer (which dominate the sub-range II) observed at a height of 10-m for the tropical cyclone Nuri in Fig. 6. The changes in eddy structures are consistent with the temperature spectrum in Fig. 8

**Fig. 7** Normalized wind-velocity component spectra vs. normalized frequency ($f = nzU^{-1}$) at the measurement height of 60-m for tropical cyclone Hagupit: **a** longitudinal wind spectra; **b** lateral wind spectra; and **c** vertical wind spectra. Note that the anomalous peak in the $S_w$ spectrum is instrumental and not physical. The conceptual model presented in Sect. 2 is also shown (*green dash lines*) for the sake of comparison

that shows high production of temperature fluctuations at the scales of 40 m near the eyewall, which is in contrast with the usual shear-convection spectrum observed in the outer vortex regions.
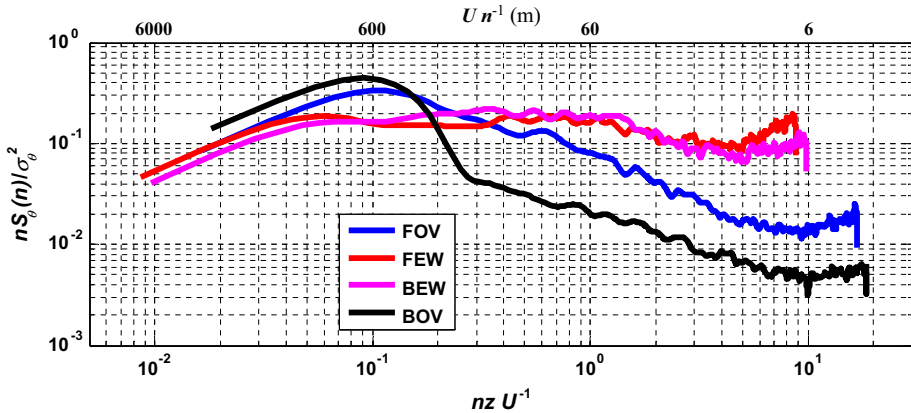
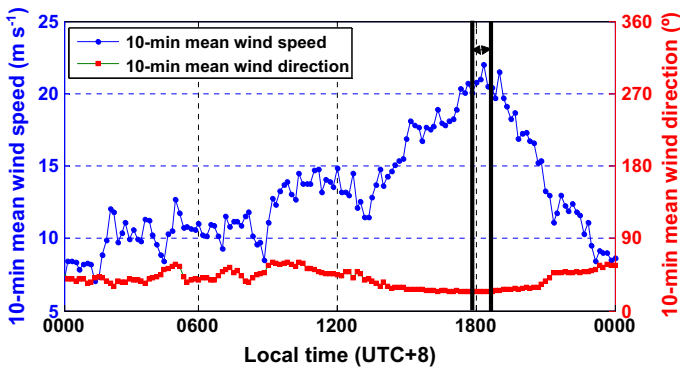**Fig. 8** Normalized temperature spectra in the tropical cyclone Hagupit at a height of 60 m



**Fig. 9** Time histories of 10-min mean wind speed and direction in tropical cyclone Chanchu at a measurement height of 10 m (the 1-h long window between the *vertical lines* has been used for estimating the spectral characteristics)

Measurements at other sites in different tropical cyclones corroborate these observations. For example, Figs. 9 and 10 summarizes an additional dataset of longitudinal wind-speed spectra estimated from measurements of fluctuating velocity components at the height of 10 m on the Red Bay tower for tropical cyclone Chanchu. The Red Bay tower is a 60-m tall tower located on the Red Bay peninsula of Shanwei City, Guangdong, China. The surrounding surface of the Red Bay tower is an open flat terrain. The sampling frequency of the sonic anemometer (CSAT3, Campbell Scientific, Inc.) was 4 Hz. Figure 9 shows the time history of the 10-min mean wind speed and direction during the period May 17–18, 2006. A dataset with duration of 1 h and mean wind speed of 21 m s$^{-1}$ was selected to analyze the wind speed spectra, as shown in Fig. 10. In Fig. 10, the blue lines are the field measured wind-speed spectra of each 10-min length segments in the 1-h long datasets. It can be noted that the field measured spectra show good agreement with the conceptual model. In sub-range I, the longitudinal spectra follow Eq. 1; the self-similarity sub-range (sub-range II) are also present; in the sub-range III, the longitudinal spectra follow the −2/3 law in the inertial sub-range. The longitudinal spectra also show significant energy in the high frequency range, and the sub-ranges IV and V exhibit features similar to the conceptual model in this study.
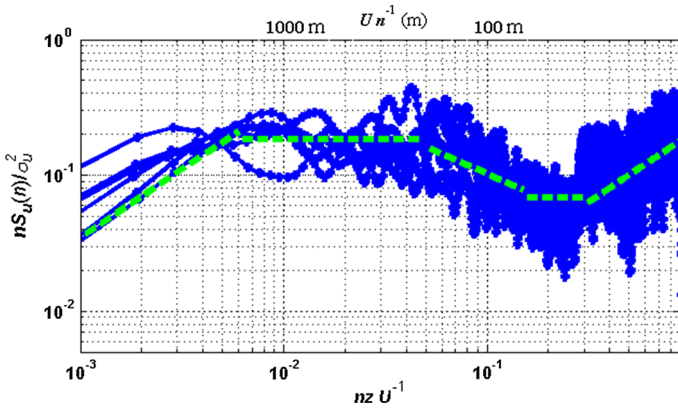
**Fig. 10** Longitudinal wind-speed spectra of the selected datasets in tropical cyclone Chanchu compared to the conceptual model (*green dash lines*)

Similar spectral features were also observed when analyzing other tropical cyclone datasets corroborating the reported observations.

## 5 Concluding Remarks

Recent measurements of velocity and temperature spectra and mean profiles in the inner and outer parts of tropical cyclones (hurricanes and/or typhoons), using coastal observation facilities, are presented here in relation to a new conceptual spectral model. This predicts how the spectra over different length scales vary with height ($z$) and radius ($r$) for the forward/backward facing regions in a tropical cyclone. It also relates the sub-ranges in the spectra to different physical processes that have been observed in the PBL over flat terrain, and also in studies where different types of turbulence can interact depending on their energy and relative length scales, e.g. Panofsky et al. (1982) and Hunt and Carlotti (2001).

Models for the various sub-ranges of the spectra are analyzed by considering detailed processes, including upscale and downscale energy transfer, and length scales in relation to the strong inhomogeneity of the turbulence. These models, which had been developed for the atmospheric boundary layer in slowly varying conditions, are applied for the first time to the structure of tropical cyclone wind spectra that change rapidly in time and space. The results are compared with recent measurements taken over a wide frequency range, and show a reasonable level of agreement.

There is, however, still insufficient data to test how the spectra of all three components of wind and of temperature vary with height and radius in tropical cyclones. There should be more detailed turbulence modelling using numerical simulations of tropical cyclones with different intensity strengths and spatial sizes. To precisely delineate the wind-speed spectrum in tropical cyclones, it is especially important to compute the effects of vertical shear, and detailed air-sea interaction processes that not only determine the mean fluxes, but also the turbulence profiles and mixing processes, with potential important practical impacts as noted in Sect. 2.

The approximate model presented here for the wind structure and turbulence spectra over a wide frequency/wavenumber range provides a method for using or extrapolating measurements to calculate unsteady and inhomogeneous wind loads on structures, ships and aircraft. They show that it is necessary to consider modifying the forms of spectra used in the

current standard codes of practice and other guides, especially when they are applied close to the eyewall (e.g. ESDU 2007).

Because winds in a tropical cyclone have a very different spatial structure from those in a typical neutrally stratified boundary layer over flat terrain, standard wind tunnels are not appropriate for simulating such airflow. A new generation of facilities capable of generating vortical flows, e.g. WindEEE laboratory (Hangan 2010) should help to improve our understanding of tropical cyclone wind structure and to simulate realistically wind loads on engineering structures.

# References

Barenblatt GI, Chorin AJ, Prostokishin VM (2005) A note concerning the Lighthill "sandwich model" of tropical cyclones. Proc Natl Acad Sci USA 102(32):11148–11150

Britter RE, Hunt J, Mumford JC (1979) The distortion of turbulence by a circular cylinder. J Fluid Mech 92(Part 2):269–301

Caracoglia L, Jones NP (2009) Analysis of full-scale wind and pressure measurements on a low-rise building. J Wind Eng Ind Aerodyn 97(5–6):157–173

Chan JCL (2005) The physics of tropical cyclone motion. Annu Rev Fluid Mech 37:99–128

Charnock H (1955) Wind stress on a water surface. Q J R Meteorol Soc 81(350):639–640

Collier JG, Thome JR (1994) Convective boiling and condensation. Oxford University Press, Oxford, 640 pp

Elghobashi S, Truesdell GC (1993) On the two-way interaction between homogeneous turbulence and dispersed solid particles. I: turbulence modification. Phys Fluids A 5(7):1790–1801

Emanuel KA (1986) An air-sea interaction theory for tropical cyclones. Part 1: steady-state maintenance. J Atmos Sci 43(6):585–604

ESDU 77032 (2007) Fluctuating loads and dynamic response of bodies and structures in fluid flows—background information. Engineering Sciences Data Unit, London

Ferrante A, Elghobashi S (2003) On the physical mechanisms of two-way coupling in particle-laden isotropic turbulence. Phys Fluids 15(2):315–329

Fitzroy R (1863) The weather book: a manual of practical meteorology. Longman, Green, Longman, Roberts, & Green, London, 464 pp

Foster RC (2005) Why rolls are prevalent in the hurricane boundary layer. J Atmos Sci 62(8):2647–2661

Hall CD, Hunt JCR, Radford AM, Carruthers DJ, Weng WS (1992) Forecasting tropical cyclones and near surface wind conditions. In: ICSU/WMO Proceeding of the international symposium on tropical cyclone disasters, Beijing, pp 232–257

Hanazaki H, Hunt J (2004) Structure of unsteady stably stratified turbulence with mean shear. J Fluid Mech 507:1–42

Hangan H (2010) Current and future directions for wind research at western: a new quantum leap in wind research through the Wind Engineering, Energy and Environment (WindEEE) Dome. Jap Assoc Wind Eng (JAWE) J 35(4):277–281

Högström U, Hunt J, Smedman A (2002) Theory and measurements for turbulence spectra and variances in the atmospheric neutral surface layer. Boundary-Layer Meteorol 103(1):101–124

Hunt J (1984) Turbulence structure in thermal convection and shear-free boundary layers. J Fluid Mech 138(1):161–184

Hunt J (2000) Dynamics and statistics of vortical eddies in turbulence. In: Proceedings conference at INI, Cambridge on vortex dynamics and turbulence. Cambridge University Press, Cambridge

Hunt J, Carlotti P (2001) Statistical structure at the wall of the high Reynolds number turbulent boundary layer. Flow Turbul Combust 66(4):453–475

Hunt J, Carruthers D (1990) Rapid distortion theory and the 'problems' of turbulence. J Fluid Mech 212(1):497–532

Hunt J, Delfos R, Eames I, Perkins RJ (2007) Vortices, complex flows and inertial particles. Flow Turbul Combust 79(3):207–234

Hunt J, Eames I, Westerweel J (2006) Mechanics of inhomogeneous turbulence and interfacial layers. J Fluid Mech 554(1):499–519

Hunt J, Kaimal JC, Gaynor JE (1985) Some observations of turbulence structure in stable layers. Q J R Meteorol Soc 111(469):793–815

Hunt J, Kaimal JC, Gaynor JE (1988) Eddy structure in the convective boundary layer—new measurements and new concepts. Q J R Meteorol Soc 114(482):827–858

Hunt J, Morrison JF (2000) Eddy structure in turbulent boundary layers. Eur J Mech B 19(5):673–694

Hunt J, Ishihara T, Worth NA, Kaneda Y (2014) Thin shear layer structures in high reynolds number turbulence: Tomographic experiments and a local distortion model. Flow Turbul Combust 92(3):607–649

Ishihara T, Kaneda Y, Hunt J (2013) Thin shear layers in high reynolds number turbulence—DNS results. Flow Turbul Combust 91(4):895–929

Kader BA, Yaglom AM (1991) Spectra and correlation functions of surface layer atmospheric turbulence in unstable thermal stratification. In: Metais O, Lesieur M (eds) Turbulence and coherent structures. Kluwer, Dordrecht, pp 387–412

Kaimal JC, Finnigan JJ (1994) Atmospheric boundary layer flows: their structure and measurement. Oxford University Press, Oxford 289 pp

Komori S, Kurose R, Takagaki N, Ohtsubo S, Iwano K, Handa K, Shimada S (2010) Sensible and latent heat transfer across the air-water interface in wind-driven turbulence. In: Proceedings of the symposium on gas transfer at water surfaces, Kyoto, pp 78–89

Lee M, Kim J, Moin P (1990) Structure of turbulence at high shear rate. J Fluid Mech 216:561–583

Li L, Xiao Y, Kareem A, Song L, Qin P (2012) Modeling typhoon wind power spectra near sea surface based on measurements in the South China sea. J Wind Eng Ind Aerodyn 104–106:565–576

Lighthill J (1998) Fluid mechanics of tropical cyclones. Theor Comput Fluid Dyn 10(1–4):3–21

Lorsolo S, Schroeder JL, Dodge P, Marks F (2008) An observational study of hurricane boundary layer small-scale coherent structures. Mon Weather Rev 136(8):2871–2893

Mann J (1994) The spatial structure of neutral atmospheric surface-layer turbulence. J Fluid Mech 273(1):141–168

Masters FJ, Tieleman HW, Balderrama JA (2010) Surface wind measurements in three Gulf Coast hurricanes of 2005. J Wind Eng Ind Aerodyn 98(10–11):533–547

Nalpanis P, Hunt J, Barrett CF (1993) Saltating particles over flat beds. J Fluid Mech 251:661–685

Owinoh AZ, Hunt JCR, Orr A, Clark P, Klein R, Fernando HJS, Nieuwstadt FTM (2005) Effects of changing surface heat flux on atmospheric boundary-layer flow over flat terrain. Boundary-Layer Meteorol 116(2):331–361

Paget AC (2009) On determining the hurricane boundary layer. Florida State University, Tallahassee FSU2374, 46 pp

Panofsky HA, Larko D, Lipschutz R, Stone G, Bradley EF, Bowen AJ, Hojstrup J (1982) Spectra of velocity components over complex terrain. Q J R Meteorol Soc 108(455):215–230

Perry AE, Abell CJ (1977) Asymptotic similarity of turbulence structures in smooth-and rough-walled pipes. J Fluid Mech 79(04):785–799

Schroeder JL, Smith DA (2003) Hurricane Bonnie wind flow characteristics as determined from WEMITE. J Wind Eng Ind Aerodyn 91(6):767–789

Smedman AS, Högström U, Hunt J (2004) Effects of shear sheltering in a stable atmospheric boundary layer with strong shear. Q J R Meteorol Soc 130(596):31–50

Smedman AS, Högström U, Hunt JCR, Sahlée E (2007) Heat/mass transfer in the slightly unstable atmospheric surface layer. Q J R Meteorol Soc 133(622):37–51

Townsend AA (1976) The structure of turbulent flow. Cambridge University Press, New York 429 pp

Wong CP, Chan PW (2010) Remote sensing observations of the subsidence zone within the eye of Typhoon Nuri in Hong Kong in 2008. Weather 65(11):299–302

Wurman J, Winslow J (1998) Intense sub-kilometer-scale boundary layer rolls observed in Hurricane Fran. Science 280(5363):555–557

Zhang JA (2010) Spectral characteristics of turbulence in the hurricane boundary layer over the ocean between the outer rain bands. Q J R Meteorol Soc 136(649):918–926

Zilitinkevich SS, Hunt J, Esau IN, Grachev AA, Lalas DP, Akylas E, Tombrou M, Fairall CW, Fernando H, Baklanov AA (2006) The influence of large convective eddies on the surface-layer turbulence. Q J R Meteorol Soc 132(618):1426–1456

Zilitinkevich SS, Hunt J, Grachev AA, Esau IN, Lalas DP, Akylas E, Tombrou M, Fairall CW, Fernando H, Baklanov A (2005) The effect of large eddies on the convective heat/mass transfer over complex terrain: advanced theory and its validation against experimental and LES data. Croatian Meteorol J 40:20–26